Hindawi Publishing Corporation
Mathematical Problems in Engineering
Volume 2012, Article ID 298685, 28 pages
doi:10.1155/2012/298685

Research Article

Research on Performance of H_2 Rich Blowout Limit in Bluff-Body Burner

Hongtao Zheng,[1] Yajun Li,[1] and Lin Cai[2]

[1] *College of Power and Energy Engineering, Harbin Engineering University, Harbin 150001, China*
[2] *Department of Power and Energy, China Ship Development and Design Center, Wuhan 430064, China*

Correspondence should be addressed to Yajun Li, fage9000@163.com

Received 19 September 2012; Revised 24 October 2012; Accepted 24 October 2012

Academic Editor: Zhijun Zhang

In order to investigate H_2 rich blowout limit at different blockage ratios and flow velocities, a CFD software FLUENT was used to simulate H_2 burning flow field in bluff-body burner, and the software CHEMKIN was adopted to analyze the sensitivity of each elementary reaction. Composition Probability Density Function (C-PDF) model was adopted to simulate H_2 combustion field in turbulence flame. The numerical results show that reactions R2 and R9 possess the largest positive and negative temperature sensitivity. Temperature has a very important influence on these two reactions. When equivalence ratio is 1, the mixture is most ignitable, and the critical ignition temperature is 1550 K. There should be an optimal blockage ratio which can stabilize the flame best. When the blockage ratio remains unchanged, the relationship between H_2 RBL and flow velocity is a logarithmic function. When the flow velocity remains unchanged, the relationship between H_2 RBL and blockage ratio is a parabolic function. A complete extinction requires three phases: the temperature sudden decline in the main stream, the energy dissipation from the recirculation zone to the main stream, and the complete extinction of the flame.

1. Introduction

Bluff-body stabilized combustion with triangular or cone stabilizers is common in afterburners of military aircraft. A central recirculation zone (CRZ) will form in the wake of the bluff-body burner [1]. The heat will diffuse to the main stream from the flame frontier. The entrainment of hot gases will improve the combustion stabilization. If the fuel concentration is ultralean or ultrarich, the heat released from the flame frontier cannot compensate that of dissipation to the main stream, and then the temperature will decrease gradually, finally inducing extinction.

Lots of researches on flame stabilized mechanism in a bluff-body burner have been carried out both in terms of experiment and theoretical treatment. Experimental researches

on this problem are extremely important, but a large-scale systematic mechanism analysis via experiments is both expensive and time consuming. The Volvo Aero Corp. [2] carried out a lot of experiments on triangular bluff-body stabilized combustion rig. Shanbhogue et al. [1] found that the flame instability is dominated by the lower intensity and the convective instability of the shear layer. He put forward that blow off will occur in multiple steps: local extinction along the flame sheer, large-scale wake disruption, and a final blow off. Frolov et al. [3] formulated a flame stabilization criterion called Michelson Criterion, according to this criterion, a flame will be blown off from the flameholder when Michelson number is <1; his result shows that there will be an optimal flame-holder size at which the best stabilization parameters were achieved. Wright [4] performed lots of experiments to define the influence of blockage on flame stabilization by bluff-bodies in ducted flow. His experiments indicated that the length of the recirculation zone varies inversely as the square root of the blockage and the flow speed past the wake increases almost linearly with blockage. He found that while the combustion was taking place, the flow speeds and flame geometry depended on the blockage ratio. However, at the flame blow off, the characteristic mechanical time is independent of that. The most important conclusion gained by Wright is that the maximum blow off speed occurs at a relatively low blockage ratio. Dawson et al. [5] found that blow off is approached by increasing the bulk velocity or decreasing the equivalence ratio. Griebel et al. [6] and Schefer [7] found that the maximum blowout velocity occurred at stoichiometric conditions. Barlow et al. [8] made use of an experimental method to study the importance of molecule diffusion and turbulence transport on flame structure. His study showed that there will be an evolution in those flames from a scalar structure dominated by molecular diffusion to one dominated by turbulent transport with Re increasing.

On the other hand, computational fluid dynamics (CFD) has been widely used to study the turbulent reacting flows, fluid machinery, and combustion systems to predict device performance and optimize their structures. Many experiment studies are used to validate the simulation accuracy and to explain the flame extinction mechanism. For example, Giacomazzi et al. [9] tested the applicability of a sub grid scale Fractal Model for LES (FM-LES) simulation of turbulent combustion by simulating a bluff-body premixed flame anchored in a straight channel. Eugenio found that 3D vortex structures periodically shortening the recirculation zone downstream of the bluff-body and entraining fresh mixture into the hot zone, this physical mechanism is involved in flame anchoring. Eriksson [2] investigated Zimont Turbulent Flame Closure Model (TFC) in conjunction with different turbulent models in simulating premixed bluff-body stabilized flame. And he found that the TFC model combined with $k-\omega$ model accurately captures the recirculation zone length and overall turbulent flame speed, the combined effect is not captured well in steady state RANS. Lin and Holder [10] studied the effects of inlet turbulent intensity and angle of attack on the chemically reacting turbulent flow and thermal fields in a channel with an inclined bluff-body flame holder. Sjunnesson [2] reported the computation of the triangular bluff-body stabilized combustion using a two-step reaction solved with Arrhenius Expression in conjunction with the Magnusen-Hjerthager combustion model and k-epsilon turbulent model. Kim et al. [11] found that LES modeling approach can reproduce the variation of recirculation zone length while the equivalence ratio changed. This approach was successfully used to assess the lean blowout condition and evaluate its behavior and physics of combustion instability. Jones and Prasad [12] adopted C-PDF/LES model to exhibit the local extinction and re-ignition in turbulent combusting and to describe the interaction between turbulence and combustion. His numerical result was in good agreement with American Sandia Flame experiment data.

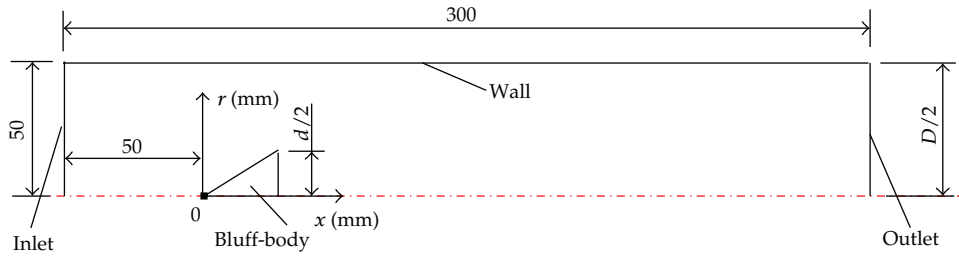

Figure 1: Geometry structure of bluff-body burner.

Even though there is a recirculation region in a bluff-body burner, the extinction will still occur if the stabilized ignition point was blown to the outside of CRZ. CRZ takes a very important effect on flammability. So the aim of the present work is to study the influence of flow velocity and blockage ratio on H_2 Rich Blowout Limit (RBL) and finally summarize a formula for H_2 RBL.

2. Geometry and Mathematical Model

Figure 1 shows the geometry of the burner with cone bluff-body and straight channel. To save the calculation expend, 2-dimension axis-symmetry model was used. Figure 2 shows the mesh adopted for the calculation domain, and the total grid number is $6.0e + 04$.

Boundary conditions: mixture inlet temperature is 293 K, inlet pressure is 1 atm and inlet velocities are shown in Table 1. The mixture is made up of H_2 and air, and the concentration of H_2 is shown in Table 5.

Outlet: pressure outlet.

Wall: adiabatic boundary.

The computations are repeated for different combinations of gas velocity and blockage ratio. The definition of Reynolds number based on the channel width has been given out as follows:

$$\mathrm{Re}_D = \frac{\rho u D}{\mu}, \tag{2.1}$$

where ρ is mixture density, u is mixture velocity, D is Channel width, μ-mixture viscosity.

The blockage ratio B is defined as

$$B = \frac{d}{D}. \tag{2.2}$$

In combustion flows, conservation equations for mass, momentum, energy, and species are solved. The standard $k-\varepsilon$ and LES models were adopted, respectively, to simulate the turbulence flow in conjunction with C-PDF and Eddy-Dissipation-Concept (EDC) combustion mode.

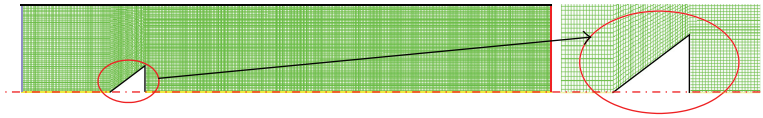

Figure 2: The calculation mesh.

Table 1: Blockage ratio and gas flow velocities (1 atm, 293 K).

Bluff-body diameter d/mm	20	30	40	50	60	70
Blockage ratio B	0.2	0.3	0.4	0.5	0.6	0.7
Gas velocity V/(m/s)	1	2	5	10	20	50
Re_D	$4.0e+3$	$8.3e+3$	$2.2e+4$	$4.4e+4$	$9.1e+4$	$2.4e+5$

Composition PDF Transport Equation (C-PDF) is as follows:

$$\frac{\partial}{\partial t}(\rho P) + \frac{\partial}{\partial x_i}(\rho u_i P) + \frac{\partial}{\partial \psi_k}(\rho \omega_k P) = -\frac{\partial}{\partial x_i}\left[\rho \langle u_i'' \mid \psi \rangle P\right] + \frac{\partial}{\partial \psi_k}\left[\rho \left\langle \frac{1}{\rho}\frac{\partial J_{i,k}}{\partial x_i} \mid \psi \right\rangle P\right]. \quad (2.3)$$

The two terms on the right-hand side represent the PDF change due to scalar convection by turbulent scalar fluxal and molecular mixing/diffusion, respectively.

The flow field researched in this paper is turbulence refer is to Re_D as shown in Table 1. Because the reaction rate highly nonlinear, modeling the mean reaction rate in a turbulent flow is extremely difficult. C-PDF is an alternative effective method to solve the premixed combustion in a turbulent flow. The principal strength of C-PDF transport approach is that the highly nonlinear reaction term is completely closed and requires no modeling. The turbulent scalar flux term is modeled by gradient-diffusion assumption. The molecular mixing/diffusion is modeled by MC, IEM, or EMST models [13]. C-PDF transport model adopts a detailed chemical mechanism for modeling the reaction rate in a turbulent flame. With an appropriate chemical mechanism, kinetically controlled species such as CO and NOx, as well as flame ignition and extinction, can be predicted by C-PDF model. Bisetti and Chen [14] adopted Join-PDF/LES approach to research Sandia Flame D, and their result showed that the prediction by EMST is quite accurate near stoichiometric, but overall trend remains unpredicted at other conditions. While Lindstedt et al. [15] found that the numerical result is in good agreement with the experiment data by MC molecular mixing model, if it turns to IEM model, it cannot capture extinction and reignition. Finally, MC molecular mixing model was used in this paper.

C-PDF transport equation cannot be solved by finite volume method; a Lagrangian Monte Carlo [13] method has been used to solve it. Because time scales of some reactions are very fast, while others are very slow, disparity of time scales results in numerical stiffness problem. It means that extensive computational load is required to integrate the chemical source term. To solve the numerical stiffness problem, in-situ adaptive tabulation (ISAT) has been employed to dynamically accelerate the chemistry calculations. Correa and Pope [16] made use of this method to calculate the burning process for one bluff-body burner, and the numerical result was in coincidence with the experiment data.

Table 2 gives out the detailed chemical mechanism of hydrogen adopted in this paper.

Table 2: Hydrogen chemistry reaction.

No.	Reaction	A_i	β_i	E_i
1	$O_2 + H \Rightarrow OH + O$	$2.000E+14$	0.00	70.30
2	$OH + O \Rightarrow O_2 + H$	$1.568E+13$	0.00	3.52
3	$H_2 + O \Rightarrow OH + H$	$5.060E+04$	2.67	26.30
4	$OH + H \Rightarrow H_2 + O$	$2.222E+04$	2.67	18.29
5	$H_2 + OH \Rightarrow H_2O + H$	$1.000E+08$	1.60	13.80
6	$H_2O + H \Rightarrow H_2 + OH$	$4.312E+08$	1.60	76.46
7	$OH + OH \Rightarrow H_2O + O$	$1.500E+09$	1.14	0.42
8	$H_2O + O \Rightarrow OH + OH$	$1.473E+10$	1.14	71.09
9	$O_2 + H + M \Rightarrow HO_2 + M$	$2.300E+18$	−0.80	0.00
10	$HO_2 + M \Rightarrow O_2 + H + M$	$3.190E+18$	−0.80	95.39
11	$HO_2 + H \Rightarrow OH + OH$	$1.500E+14$	0.00	4.20
12	$HO_2 + H \Rightarrow H_2 + O_2$	$2.500E+13$	0.00	2.90
13	$HO_2 + OH \Rightarrow H_2O + O_2$	$6.000E+13$	0.00	0.00
14	$HO_2 + H \Rightarrow H_2O + O$	$3.000E+13$	0.00	7.20
15	$HO_2 + O \Rightarrow OH + O_2$	$1.800E+13$	0.00	−1.70
16	$H + H + M \Rightarrow H_2 + M$	$1.800E+18$	−1.00	0.00
17	$OH + H + M \Rightarrow H_2O + M$	$2.200E+22$	−2.00	0.00
18	$O + O + M \Rightarrow O_2 + M$	$2.900E+17$	−1.00	0.00
M	$H_2O/6.5\ O_2/0.4\ N_2/0.4/$		Third body efficiency	
Unit	A_i-cm · mole · s · K, $\beta_i - 1$, E_i-kJ/mole.			

3. Validations of Mathematical Model

3.1. Validations of Independence of Grid Size and Time Step

The studies on grid size and time step independence have been performed to determine the optimal grid and time step with a good accuracy for the simulation. Also, the k-epsilon-C-PDF model was used.

Table 3 gives out the grid size range which changes from 0.5 mm to 2.0 mm (the grid number varies from $1.0e+05$ to $1.6e+04$). The time step is, respectively, 0.05 ms, 0.10 ms, 0.20 ms, and 0.50 ms, as shown in Table 4. The average temperatures on section $x = 150$ mm and $x = 350$ mm were adopted to verify the accuracy of grid size and time step. Table 3 shows that on section $x = 150$ mm, the average temperature at grid size $\Delta = 1.0$ mm is only 1°C higher than that at grid size $\Delta = 0.5$ mm. On section $x = 350$ mm, the average temperature at grid size $\Delta = 1.0$ mm is 13°C higher than that at grid size $\Delta = 0.5$ mm. So, the numerical simulation is independent when grid size is $\Delta = 1.0$ mm (the grid number is $6.0e+04$). Table 4 shows that on section $x = 350$ mm, the maximum temperature error is only 20°C between time step 0.1 ms and 0.05 ms. So, when the time step is 0.1 ms, the numerical result does not rely on it.

Figure 3 shows the temperature curves at different grid size and time step. It indicates that when the grid size is 1.0 mm and the time step is 0.1 ms, the temperature error between the numerical result and the experiment data is extremely small. So, it can be included from the results that the optimal grid size is $\Delta = 1.0$ mm and the optimal time step is $\Delta t = 0.1$ ms.

Table 3: Grid size independence validation with time step 0.1 ms.

Grid size/mm	$\overline{T_{x=150}}$/K	ΔT/K	$\overline{T_{x=350}}$/K	ΔT/K	Grid amount
0.5	419	—	768	—	$1.0e+05$
0.8	420	1	760	8	$9.2e+04$
1.0	420	1	755	13	$6.0e+04$
1.5	415	4	707	61	$2.8e+04$
2.0	414	5	666	102	$1.6e+04$

Table 4: Time step independence validation with grid size 1.0 mm.

Time step/ms	$\overline{T_{x=150}}$/K	ΔT/K	$\overline{T_{x=350}}$/K	ΔT/K	Remark
0.05	424	—	775	—	—
0.10	419	5	755	20	Independent
0.20	405	14	707	68	Worse
0.50	402	22	604	171	Worse

3.2. *Experiment Validation for Model Accuracy*

Figure 4 shows the combustion device of Volvo Aero Corp. triangular bluff-body which has been widely used to research the flame stabilization mechanism both in terms of experiments and theoretical data. Over the years, many CFD researches relied on the experiment data of this device have been carried out to investigate its stabilized mechanism [2]. In order to validate the accuracy of the mathematical model, this combustion rig was used with Smagorinsky-Lily-LES-EDC (SL-LES-EDC) model, k-epsilon-EDC model, and k-epsilon-C-PDF model.

Geometry model and boundary conditions are as follows:

Length × width × height = 660 × 240 × 120 mm;

Side length of bluff-body with the equilateral triangular cross-section: 40 mm;

Inlet condition of mixture of air and propane: $T = 288\,\mathrm{K}$, $V = 17\,\mathrm{m/s}$, $p = 1\,\mathrm{atm}$, mass flow rate is 0.6 kg/s, equivalence ratio is $\phi = 0.65$;

Outlet: pressure outlet;

Wall: adiabatic boundary;

Fuel oxidation was modeled by one-step global reaction:

$$C_3H_8 + 5O_2 \Rightarrow 3CO_2 + 4H_2O \tag{3.1}$$

The reaction rate is that proposed by Fluent Database according to Arrhenius Law [9].

$$\dot{\omega} = \frac{d[C_3H_8]}{dt} = -4.836 \times 10^{-9} e^{-15100/T} \times [C_3H_8]^{0.1}[O_2]^{1.65}. \tag{3.2}$$

The Reynolds number based on the bluff-body burner device and on the velocity at the bluff-body location is about 10^5. The flow field is simulated using compressible N-S equations.

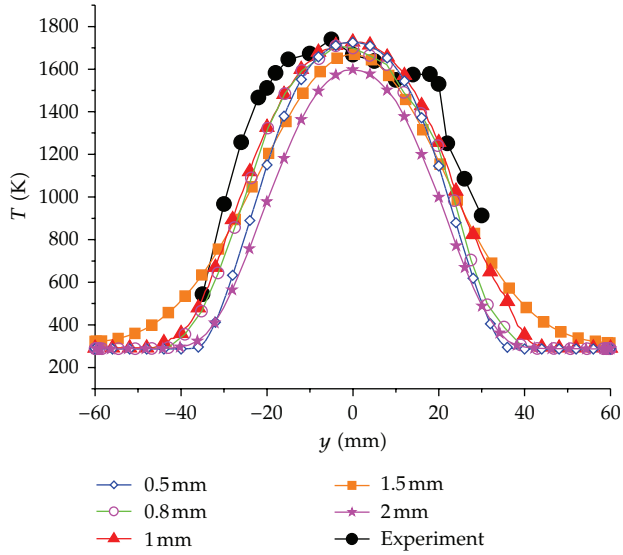

(a) Grid size independence

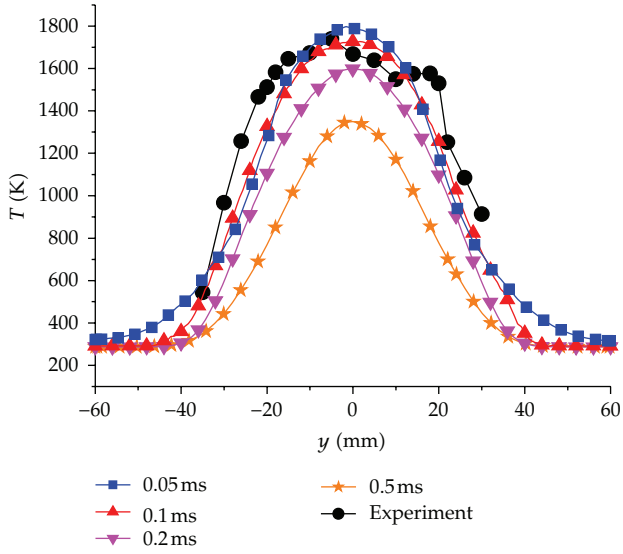

(b) Time step independence

Figure 3: Profiles of temperature on section x = 150 mm at different grid size and time step.

Figures 5, 6, and 7 show the comparison between numerical results and the experiment data. The results indicate that SL-LES-EDC model will overpredict the recirculation length and underestimate its width. Giacomazzi et al. [9] found that FM-LES-EDC model can accurately predict the recirculation zone position, but in combustion flow field, it will underestimate the velocity nearby the channel wall, and it may be because of the disadvantage of the FM-LES-EDC in dealing with the turbulent viscosity nearby the channel wall. Relatively, the k-epsilon-C-PDF, k-epsilon-EDC, and SL-LES-EDC models can predict the velocity better than FM-LES nearby the channel wall.

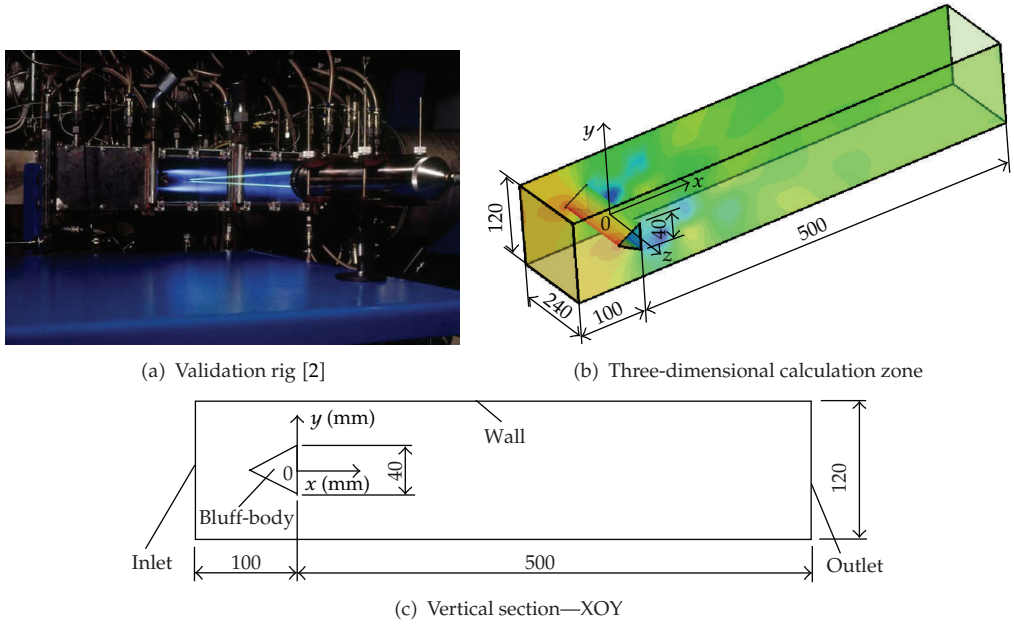

(a) Validation rig [2]

(b) Three-dimensional calculation zone

(c) Vertical section—XOY

Figure 4: Validation rig and calculation zone geometry.

Figures 7 and 8(b) show that in reacting case, SL-LES-EDC model will overestimate the flame width and the temperature in the flame zone. The maximal temperature of the flame from SL-LES-EDC is 400 K higher than that of the experiment data. The k-epsilon-EDC model will also overestimate the temperature in the flame center, but it will underestimate the flame temperature at the outside of the flame zone (see Figures 7 and 8(c)). Figure 7 shows that FM-LES-EDC can relatively accurately predict the flame temperature, except for the maximal temperature, and it will overestimate its value about 100 K. In spite of this situation, it can reproduce the flame vortex structures and the flame periodic fluctuation. Compared with FM-LES-EDC model, k-epsilon-C-PDF can predict the flame temperature more accurately but it cannot capture the flame vortex shell accurately.

In a word, the agreement observed between k-epsilon-C-PDF model result and published classics experiment data is acceptable. The k-epsilon-C-PDF combustion model can accurately predict the flame temperature, while SL-LES-EDC model can accurately predict the vortex structures and explain the extinction mechanism.

Figure 9 shows the comparison of recirculation zone between cold field and combustion field based on k-epsilon-C-PDF model. The figures indicate that the performance of recirculation zone of combustion field is apparently different from that of the cold flow. The recirculation length of combustion field is about two times more than that of the cold flow. This should be attributed to the flame fluctuation and the dramatic heat releasing from chemistry reaction. The flame propagation extends the axis momentum of the velocity and lengthens the recirculation zone further downstream from the bluff-body.

Figure 10 shows the streamlines of cold field and combustion field from SL-LES-EDC model and k-epsilon-CPDF model. The results show that, in the cold field, SL-LES-EDC model can capture the asymmetric von Karman vortex street at the wake zone of the bluff-body. The period of the vortex shedding is 110 Hz, in agreement with the measurements

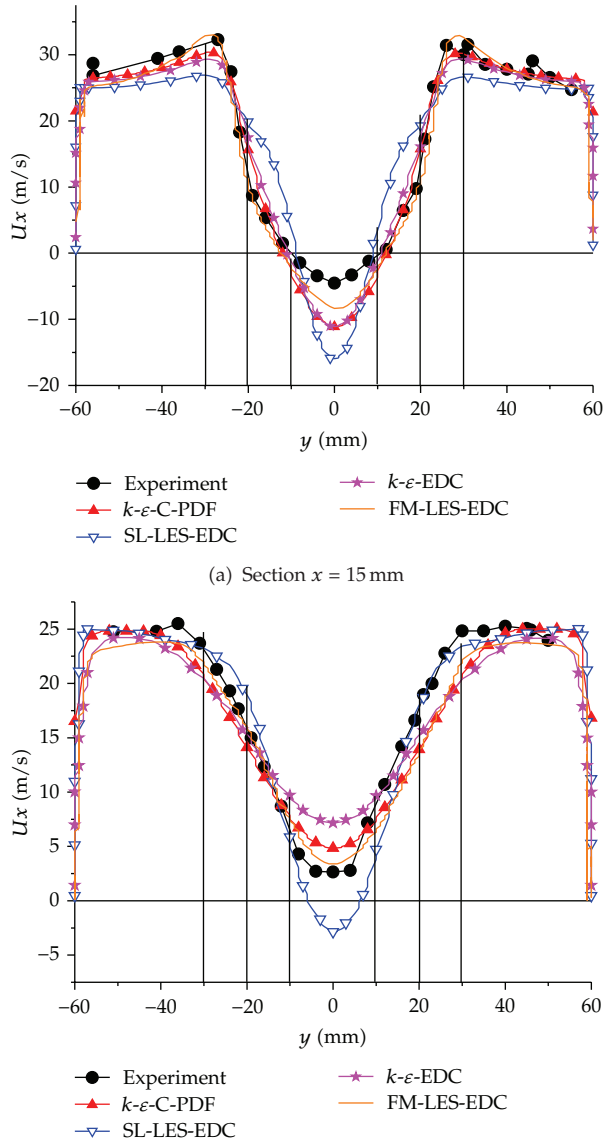

(a) Section $x = 15$ mm

(b) Section $x = 61$ mm

Figure 5: Profile of Ux of cold field at sections (a) $x = 15$ mm, (b) $x = 61$ mm.

(105 Hz) [9]. The asymmetric von Karman shedding of coherent vortices no longer exists in the reacting case. Shanbhogue et al. [1] attributed this absence of Karman vortex street for reacting case to the dilatation effect of the heat release. However, what can be concluded from the numerical simulation is that the asymmetric Karman Vortex Street does not disappear in the reacting case, it just converges with the downstream nearby the bluff-body, and the direction of the vortex at the wake zone is still also changed periodically.

Figure 10 shows that k-epsilon turbulent model cannot capture the asymmetric von Karman vortex street shedding, while the model can just capture the central recirculation zone after the flameholder. Also, in the cold field, k-epsilon model can predict the velocity

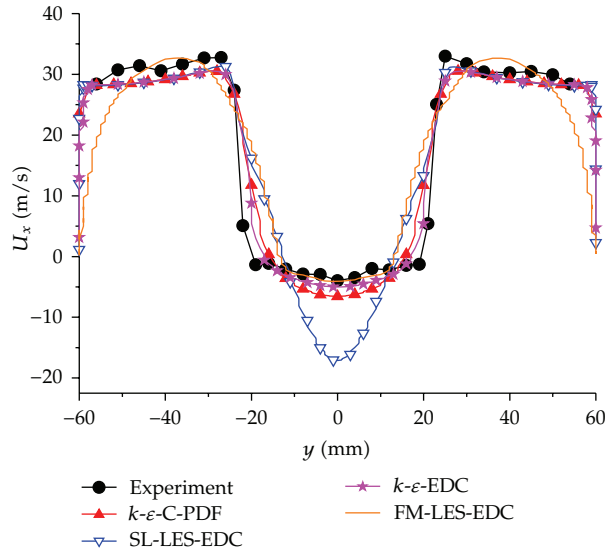

(a) Section x = 15 mm

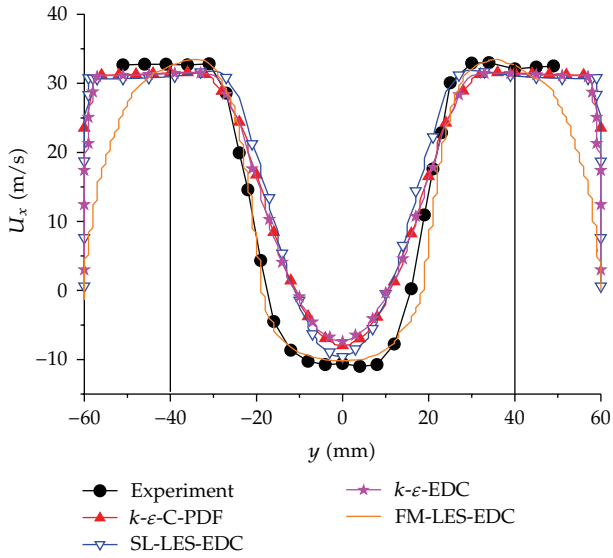

(b) Section x = 61 mm

Figure 6: Profile of Ux of combustion field at sections (a) x = 15 mm, (b) x = 61 mm.

fluctuation like "a polliwog tail" alternation periodically. That is because the dilatation effect of the heat releases possessing the dominant influence than the fluctuation of Karman Vortex Street. Figure 11 gives out an image of a combustion experiment based on a triangular bluff-body [1].

Figure 12 shows the extinction process of the triangular bluff-body combustion field. What can be included from the numerical is that the entire extinction process experiences three phases: (1) the appearance of discontinuous flame; (2) the flame local extinction and reignition in the recirculation zone; (3) global extinction.

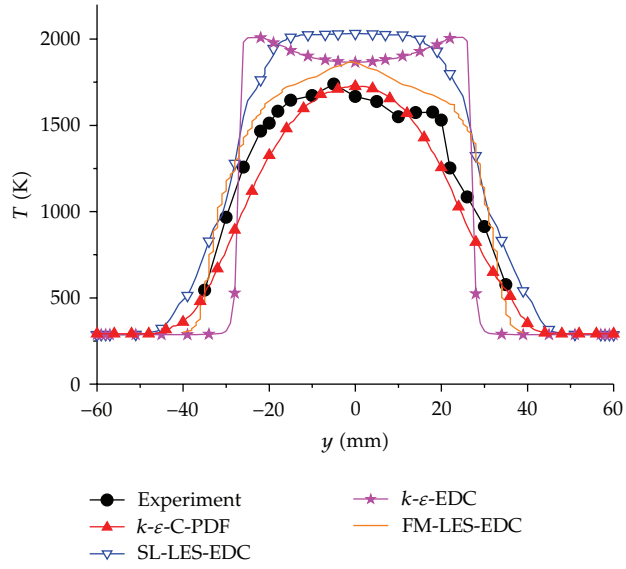

(a) Section $x = 150$ mm

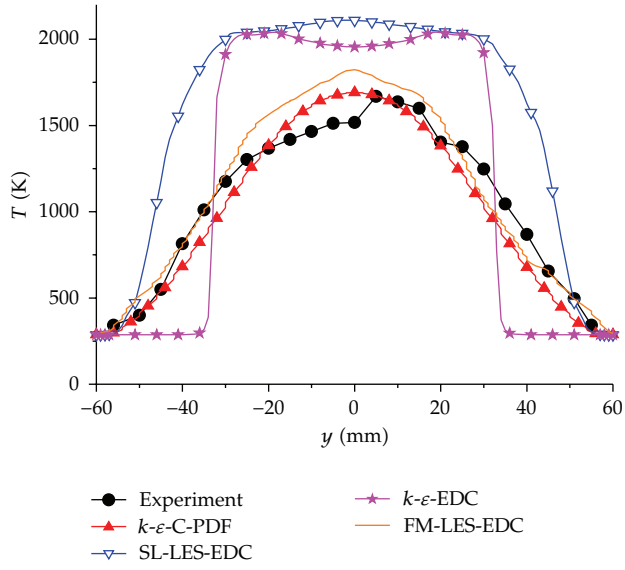

(b) Section $x = 350$ mm

Figure 7: Profiles of temperature at sections (a) $x = 150$ mm, (b) $x = 350$ mm.

(1) Discontinuous flame: when the equivalence ration is close to blow off, the flame temperature would decline rapidly, chemistry reaction would be slower, and the heat transfer and dissipation to the flame sheet can ignite the fresh mixture and, finally, induce the discontinuous flame. The first discontinuous position presents at the recirculation zone stagnant point.

(2) Local extinction and reignition: if the cold mixture is heated up and reignited by flame kernel exactly, the flame is at critical blowout limit state of being acute and

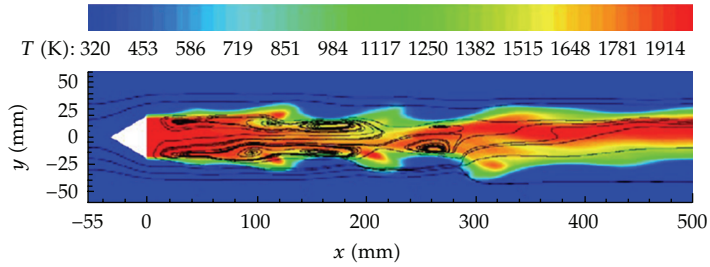

(a) Temperature field from Eugenio by FM-LES-EDC [9]

(b) Instantaneous temperature by SL-LES-EDC model

(c) Instantaneous temperature by k-epsilon-EDC model

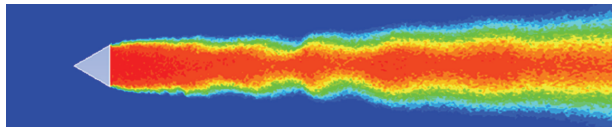

(d) Instantaneous temperature by k-epsilon-C-PDF model

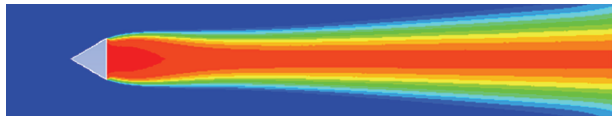

(e) Mean temperature by k-epsilon-C-PDF model of 10 periodic

Figure 8: Comparison of temperature field by different mathematical model.

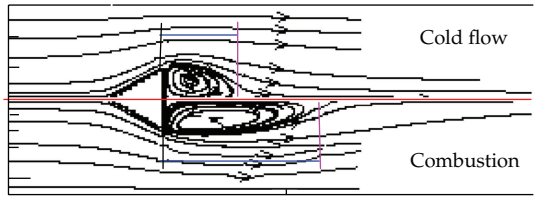

(a) Streamline

(b) $Ux = 0$ interface

Figure 9: Comparison of recirculation zone between cold flow and combustion field.

unstable. The local extinction and reignition will alternately appear in the recirculation zone. During the blow off, significant fragmentation of the flame occurred, with branches of flame remaining anchored in the bluff-body wake zone.

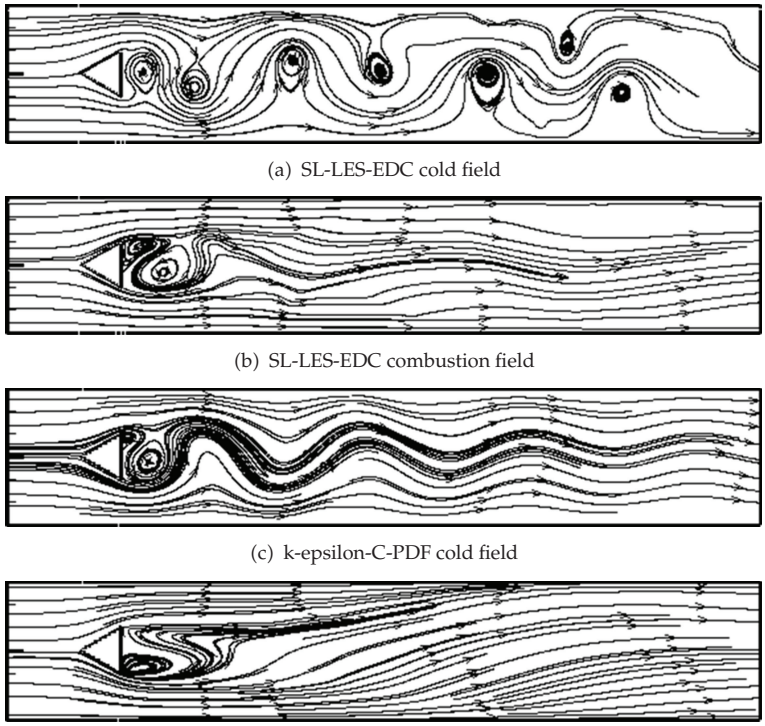

(a) SL-LES-EDC cold field

(b) SL-LES-EDC combustion field

(c) k-epsilon-C-PDF cold field

(d) k-epsilon-C-PDF combustion field

Figure 10: Streamline of cold flow field and combustion field.

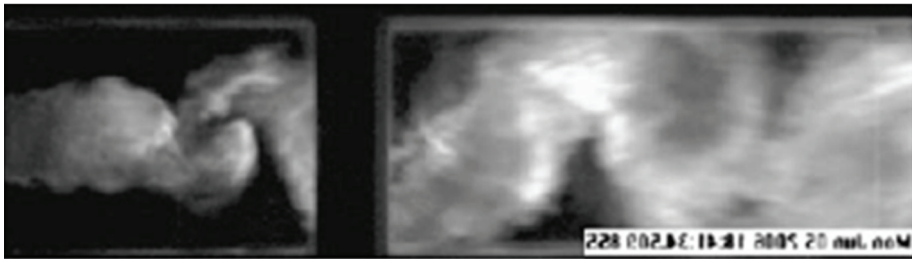

Figure 11: Image of combustion experiment [1].

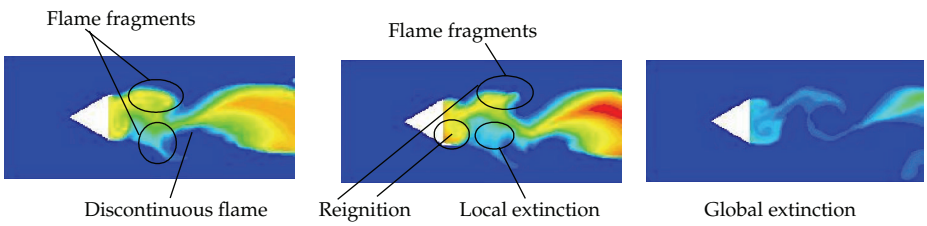

(a) Discontinuous flame (b) Local extinction and reignition (c) Global extinction

Figure 12: Extinction process.

(3) Global extinction: the fame pockets moved to the downstream of the recirculation and finally induced the global extinction. Overall blow off occurred with the gradual elimination of these flame fragments and local extinction [1].

4. Result and Analysis

4.1. Hydrogen Rich Blowout Limit

H_2 RBL is defined as the mole fraction of H_2 in the mixture. It is the H_2 mole concentration limit beyond which the extinction will occur. So, it is dimensionless (%) consider

$$\text{RBL} = \frac{n_{H_2}}{n_{\text{mixture}}}, \tag{4.1}$$

where, n_{H_2}-mole flow rate of H_2 in mixture, n_{mixture}-mole flow rate of mixture. Because the higher H_2 RBL means the wider operation range and the mixture species can change in a wider range. And it is beneficial for the bluff-body burner, so it is interesting to find a way to improve H_2 RBL.

Table 5 and Figure 13 show the numerical results of H_2 RBL at different blockage ratio and gas velocities. It can be found that when blockage ratio remains unchanged, H_2 RBL decreases as gas flow velocity is increased. The increasing of the gas velocity will enhance the flow fluctuation and the turbulence intensity, at the same time, the convection and conduction between reactant and product will be improved, and the burning will be enhanced. But when the gas velocity is too large, the flame is close to blowout limit, the turbulence fluctuation will affect the flame's propagation greatly near blowout flames. There will be more and more burning mass which will penetrate into the cooling mixture, at the same time, fresh reactants will penetrate through the CRZ from the flame forward region and abundant of flame fragments will occur, then the separate flame fragments will move randomly inside the CRZ or cooling mixture. When the heat released from chemical reaction is not sufficient to maintain its burning, the flame local extinction will occur. In a word, the main reason of flame blow-out is the generation and elimination of the flame fragments caused by gas velocity increase. So the flame blow out will be approached by increasing the gas velocity, and increasing the mainstream velocity has an adverse effect on flame flammability. This conclusion is accordance with that of EL-feky and Penninger [17] and Dawson's [5] experiment result. Shanbhogue [1] also found that temporally localized extinction occurred sporadically on near blow off flames. Under certain conditions the flame cannot persist indefinitely when Re is too large. The number of local extinction per unit time increase as blow off is approached, and the ultimate blow off event results from more and more local extinction. His conclusion does also support the conclusion summarized in this paper, and the numerical results from the present work are in accordance with his conclusion.

Table 5 and Figure 13 also show that when the gas velocity remains unchanged, the H_2 RBL will rise first and decline later as the blockage ratio is increased. It means that there will be an optimal blockage ratio (in the present work, the optimal blockage ratio is $B = 0.5$, as shown in Figure 13(b)) which can stabilize the flame best. Also at the optimal blockage ratio, the H_2 RBL will reach the largest value. Blockage ratio has a very important effect on the flame geometry, flow speeds, and CRZ length which will influence the flame stability greatly. When the blockage ratio is increased, both the length of CRZ and the gas velocity at the bluff-body channel will increase rapidly. However, they have an opposite effect on H_2 RBL; for

Table 5: H_2 RBL (volume concentration).

V	B					
	0.2	0.3	0.4	0.5	0.6	0.7
1	0.775	0.782	0.783	0.786	0.779	0.777
2	0.765	0.775	0.774	0.776	0.770	0.767
5	0.753	0.763	0.763	0.765	0.757	0.754
10	0.745	0.755	0.753	0.754	0.749	0.746
20	0.735	0.743	0.743	0.745	0.740	0.737
50	0.723	0.728	0.728	0.731	0.725	0.724

example, the H_2 RBL will rise as the length of CRZ is increased, while it will decrease as the gas velocity is increasing. As a result, there would be an optimal blockage ratio. So, the curves in Figure 13(b) are concave. Frolov et al. [3] have carried out the same conclusion about the optimal bluff body diameter by numerical simulation and experiment. Wright [4] found that the maximum blow off speed will occur at $B = 0.35$ for flat-plate flame-holders. He found that the blockage ratio has a very important effect on the flame geometry, flow speeds, and CRZ length which will influence the flame stability greatly.

In a word, the H_2 RBL will be improved by decreasing the gas velocity, or by increasing the blockage ratio before the optimal value. But if the blockage ratio increases when it has exceeded the optimal value, the H_2 RBL will decline. So, when the surroundings remain unchanged in bluff-body burner, the H_2 RBL is a function of gas flow velocity and blockage ratio. To investigate the relationship between gas flow velocity, blockage ratio, and H_2 RBL, the gas velocity has been denoted by logarithmic coordinates (named, logarithmic velocity-lg$V$) as shown in Figure 14(a). It can be seen that the function relationship between H_2 RBL and lg$V$ is nearly linear. The H_2 RBL will linearly decline with the increase of lg$V$, so the H_2 RBL fitting formula could be assumed as follows:

$$Y = a\lg V + b \quad (a, b\text{-undetermined coefficient}). \tag{4.2}$$

Linear fitting of the numerical data results by Least Square Method, and the value of a, b can be gained as shown in Table 6. Figure 14(b) shows the numerical results and the fitting curve originated from fitting formula when $B = 0.3$. It can be concluded that the errors between the numerical results and fitting curve are very small, which means that the assumption of H_2 RBL is acceptable.

Figure 15 shows the relationship between a or b and B. Table 6 and Figure 15 show that as the blockage ratio increases, the slope a will increase first and decrease later, while the intercept b will decrease first and increase later. The relationship between a or b and B is approximately a quadratic function, so the formula for a, b and B can be assumed as follows:

$$\begin{aligned} a &= m_0 + m_1 B + m_2 B^2, \\ b &= n_0 + n_1 B + n_2 B^2. \end{aligned} \tag{4.3}$$

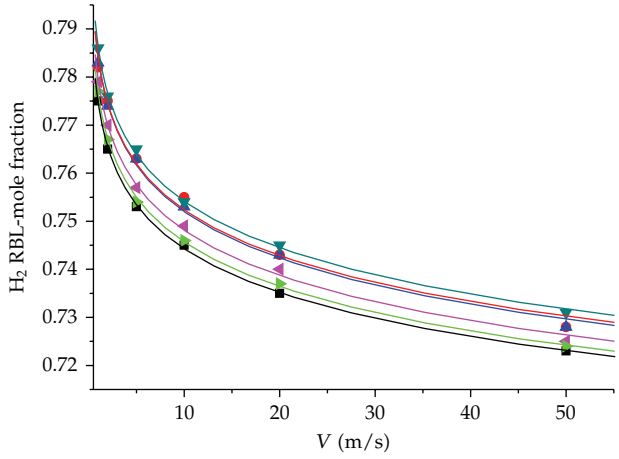

(a) Linear coordinate

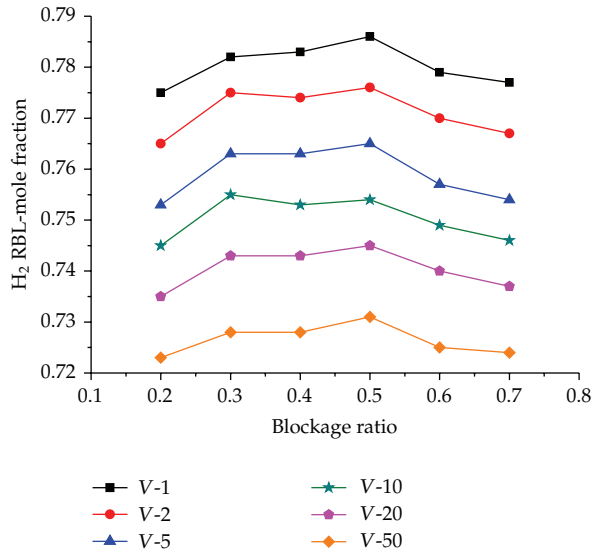

(b) Curves of H_2 RBL versus blockage ratio

Figure 13: H_2 RBL versus gas flow velocity and blockage ratio.

Fitting the curve with a quadratic function by Least Square Method, then a formula for a, b and B can be summarized as follows ($V \leq 50\,\mathrm{m/s}$):

$$a = -0.02646 - 0.025088B + 0.027977B^2,$$
$$b = 0.75327 + 0.145B - 0.1625B^2. \tag{4.4}$$

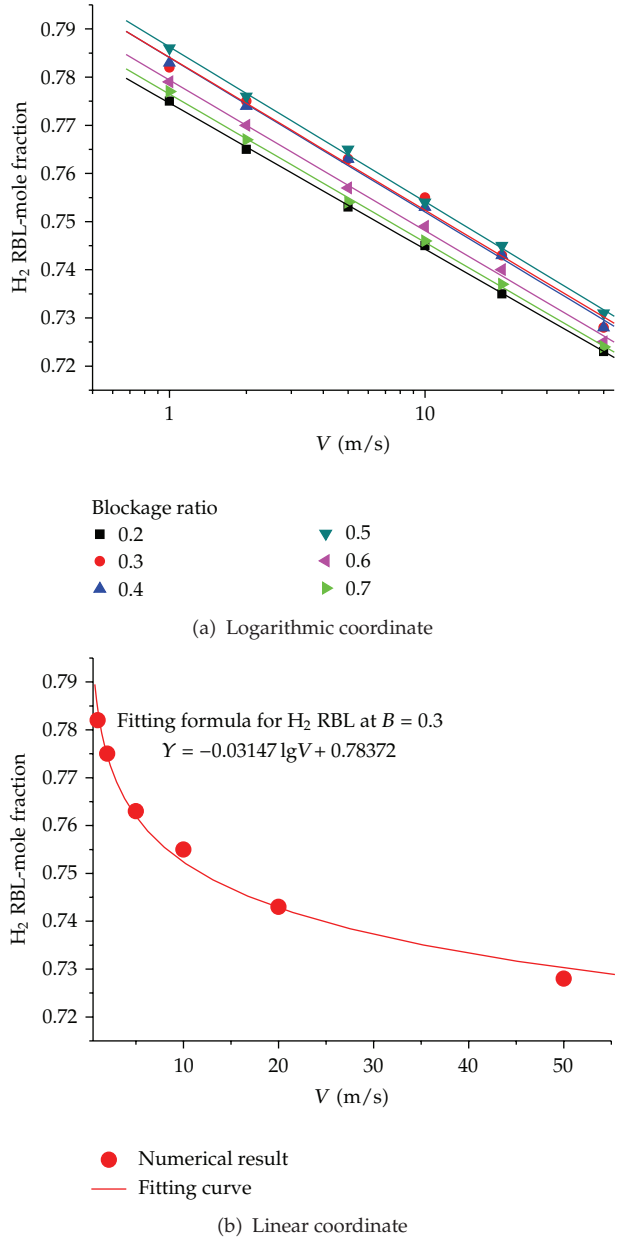

Figure 14: Curves of H_2 RBL versus gas flow velocity and fitting curve (the symbols are numerical results and the lines originate from the fitting formula).

Figure 16 shows that the distance from the bluff-body to the recirculation center will increase as the blockage ratio increases, and so does the recirculation length. But while the blockage ratio remains unchanged, the position and length of the recirculation region is unchanged, no matter how large the flow velocity is. It means that blockage ratio significantly influences the recirculation region length. Wright [4] found that when the situation is approaching to blow off, the residual flame occupies just the recirculation zone region, and the recirculation-zone length remains unchanged. Only the blockage has a strong influence

Table 6: Fitting formulas about H_2 RBL and gas flow velocity.

B	RBL fitting formula/100%
0.2	$Y = -0.03035 \lg V + 0.77462$
0.3	$Y = -0.03147 \lg V + 0.78372$
0.4	$Y = -0.03205 \lg V + 0.78404$
0.5	$Y = -0.03212 \lg V + 0.78627$
0.6	$Y = -0.03125 \lg V + 0.77937$
0.7	$Y = -0.03080 \lg V + 0.77650$

on recirculation-zone length. For a given blockage ration, the wake with after the bluff-body is virtually constant, independent of mixture ratio and flow speed. So, people cannot judge the blowout limit just by recirculation length.

4.2. Ignition Process Analysis

The simulation of ignition process is done in the condition of $d = 30$ mm, $V = 2$ m/s, and equivalence ratio $\phi = 0.5$. A small zone is patched with high temperature, so the burning will begin. With the development of ignition process, the flame flied becomes stable after $t = 200$ ms, and the calculation of ignition process continues to $t = 500$ ms for ensuring the stability of the flow field. When $t = 500$ ms, reduce the H_2 volume concentration to 0.095 ($\phi = 0.25$, below the H_2 RBL) to simulate the extinction process.

Start ignition: $t = 0$ ms (equivalence ratio is $\phi = 0.5$);

Ignition process: $t = 0$–500 ms;

Extinction process: $t = 500$–1400 ms (equivalence ratio is $\phi = 0.25$).

First half parts of Figure 17 (before the vertical dash line) and Figure 18(a) show the species mass fraction and temperature distribution of section $x = 40$ mm in ignition process. When $t = 100$ ms, the average temperature of section $x = 40$ will increase sharply, so does the mass fraction of H_2O, OH, O, H, while the mass fraction of hydrogen and oxygen will decrease greatly, these phenomena mean that the flame has been ignited at this time. In the period of 100 ms to 200 ms, the average temperature of section $x = 40$ mm will decrease suddenly, and meanwhile, the mass fraction of H_2O, OH, O, and H will also decrease, and then remain unchanged. The concentration of H_2 and O_2 would rebound after $t = 100$ ms, and this means that the flame is not stable until $t = 200$ ms, so it can be seen that the ignition sequence is not successful until $t = 200$ ms.

Figure 18(a) shows the temperature field of whole ignition process. There is a fluctuation of the flame during ignition process as shown in Figures 17 and 18(a) This is mainly because when the burning has just taken place first in CRZ, a large amount of combustion and intermediate products generated with heat releasing from chemical reaction, but the heat and the intermediate products cannot spread to the main stream immediately, and they would accumulate rapidly at this time. While $t = 100$ ms, the remainder reactants and the accumulated intermediate products have almost been consumed completely. In order to maintain burning, fresh reactants are required, and at this moment, the heat which spread to the main stream from recirculation zone is more than the heat released from burning, so the temperature and the chemical reaction in the recirculation zone will decline. When $t = 200$ ms, the heat released from fresh burning in the recirculation zone is adequate to compensate for the heat taken away by the main stream, and up to now, the combustion is steady.

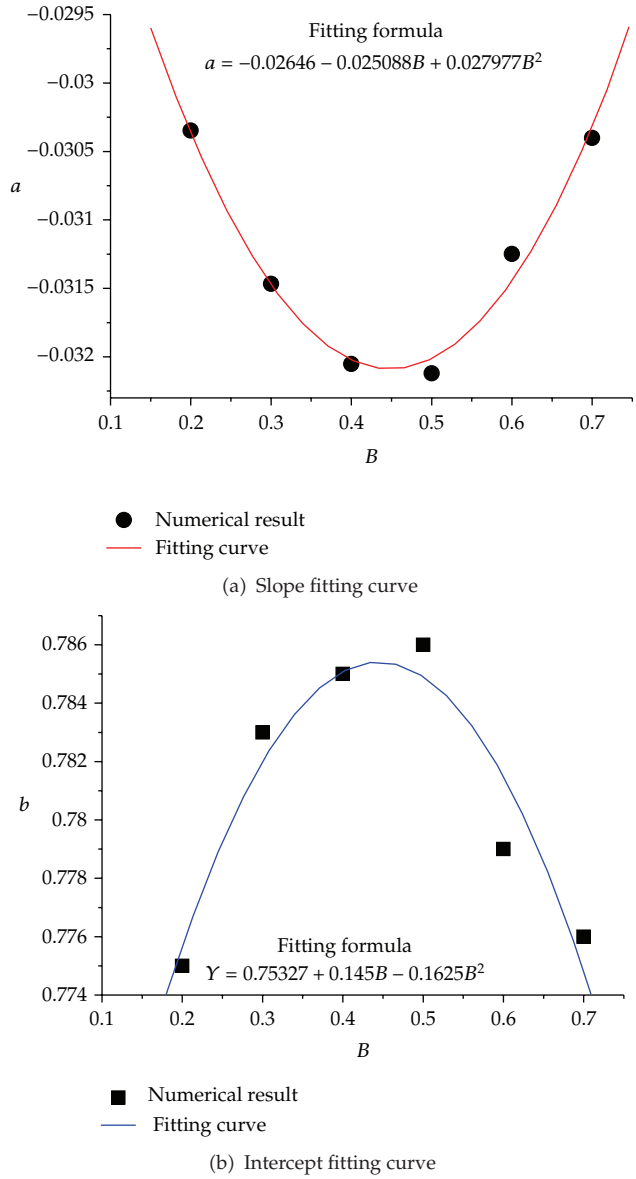

(a) Slope fitting curve

(b) Intercept fitting curve

Figure 15: Slope and intercept of fitting function of H_2 RBL versus blockage ratio B.

It can be concluded that a successful ignition sequence in a bluff-body burner requires three phases: (1) the startup of ignition in the recirculation zone; (2) the energy accumulation in the recirculation zone; (3) the flame propagation from the recirculation zone to the main stream.

4.3. Extinction Process Analysis

When $t = 500$ ms, in order to investigate the flame extinction process, hydrogen concentration was reduced to 0.095 (lower than the flammable limit), and the extinction will happen.

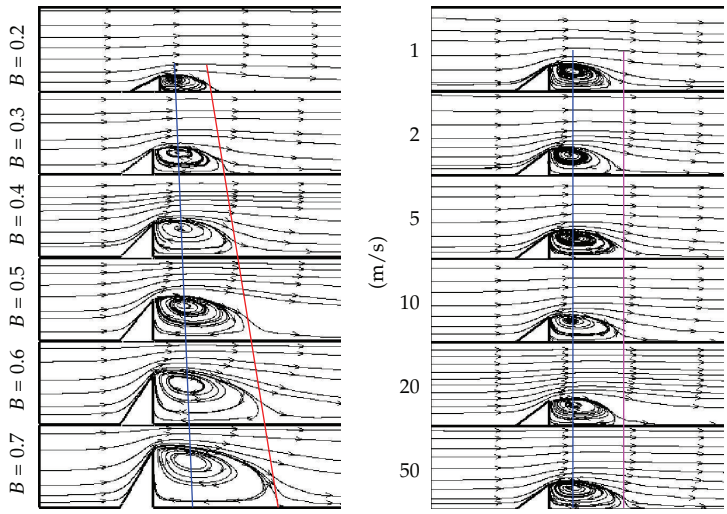

(a) Recirculation versus blockage ratio

(b) Recirculation versus flow velocity

Figure 16: Streamlines of recirculation zone.

Latter half parts of Figure 17 (after the vertical dash line) show that it takes about 100 ms for the whole combustion field to reduce H_2 mass fraction to the new value 0.095. It can be seen from Figure 17 that the whole extinction process takes about 600 ms, which is longer than ignition. When t = 600 ms, the fresh mixture has reached the CRZ completely, and the gas concentration in the recirculation is below the flammable limit, but the flame does not extinguish immediately, this is because the energy dissipation from the recirculation zone to the main stream is slow, so the temperature in the recirculation zone is still high enough to maintain the burning for a while, and the flame will not extinguish until the energy in the recirculation totally diffuse to the main flow after the temperature in the recirculation zone reduces to the extinguish level, and the flame goes out totally as Figure 18(b) shows.

During t = 600–800 ms, the temperature attenuation rate would reach a new value, meaning that the burning is still going on below H_2 RBL, and the flame length would reduce gradually. When t = 800–1400 ms, the average temperature will slowly decrease to the cold field level, this process is the burning of remaining gas in the recirculation. So far, the flame has extinguished completely. Figure 18(b) shows that the flame will take an "M" shape with reaction fronts inside the CRZ near the blow off condition. This flame shape is in well agreement with that gained by Dawson et al. [5] in their experiment measurement.

In a word, C-PDF model is accurate enough to capture the flame extinction. In terms of control of marine power, it can be concluded that the flame will extinguish as soon as the average temperature is lower than that at 800 ms. Feedback should be provided to fuel and air control system promptly to regulate fuel supply in order to avoid extinction.

So, a complete flame extinction process requires three phases: (1) the sudden decline of temperature in the burner because of the decline of fuel concentration; (2) the energy dissipation from the recirculation zone to the main stream; (3) the flame complete extinction.

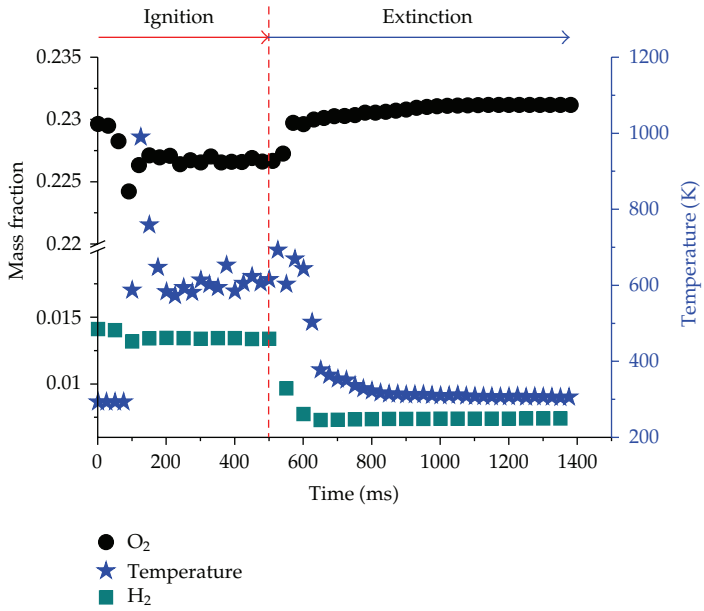

(a) O_2, H_2, Temperature

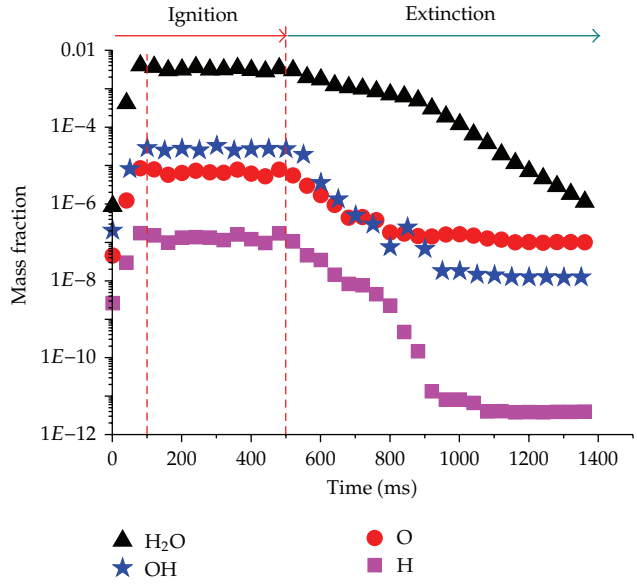

(b) H_2O, OH, H

Figure 17: Profiles of species average mass fraction and average temperature on section $x = 40$ mm versus time from ignition (0–500 ms) to extinction (500–1400 ms).

4.4. Sensitivity Analysis for Chemistry Reaction

The sensitivity analysis is a powerful tool in interpreting the results of computational simulations, and it can be used to research the influence of temperature, species concentration, and equivalence ratio on each elementary reaction [18, 19]. Rate-of-production analysis provides

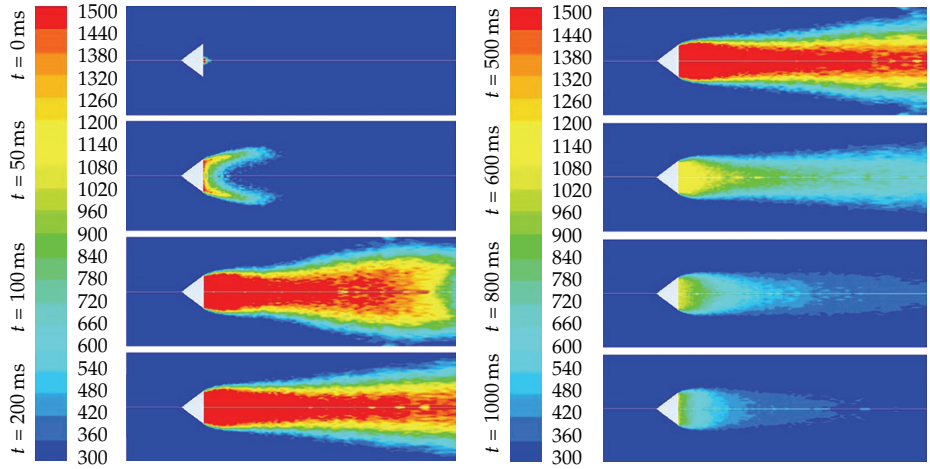

(a) Ignition process (b) Extinction process

Figure 18: Temperature distribution from ignition process to extinction process.

complementary information on the direct contributions of individual reactions to species net production rates.

To investigate the contribution of each elementary reaction to H_2 burning, the software CHEMKIN [18] was used to analyze the first-order sensitivity coefficient of temperature and species according to the H_2 18 steps reaction mentioned earlier in the paper. Finally, make use of sensitivity coefficient to investigate the ignition and extinction process. CHEMKIN assumes a variable Z as

$$\frac{dZ}{dt} = F\left(Z, t, \vec{a}\right), \tag{4.5}$$

where $Z = (Y_1, Y_2, \ldots, Y_k)^T$ are standards for mass fraction of each species, $\vec{a} = (A_1, A_2, \ldots, A_N)$-preexponential factor of each species, and the first-order sensitivity coefficient is defined as

$$\begin{aligned} w_{l,i} &= \frac{\partial Z}{\partial a_i}, \\ \frac{dw_{l,i}}{dt} &= \frac{\partial F_l}{\partial Z} \cdot w_{l,i} + \frac{\partial F_l}{\partial a_i}. \end{aligned} \tag{4.6}$$

For heat-of-formation sensitivity, $\vec{a}$ represents the vector of heats of formation for all the species in the system. The change of $\vec{a}$ will bring in the species concentration variety. The bigger sensitivity coefficient means the more significant influence caused by $\vec{a}$.

The equivalence ratio for calculation case in Figure 19 to Figure 23 was 1. Figure 19 shows that reaction R2 possesses the largest positive temperature sensitivity coefficient other than all the other elementary reactions. The sensitivity coefficient reaches the peak value at 1550 K. It indicates that at $T = 1550$ K, a little temperature variation will induce a large chemistry reaction rate change for R2 and R9. So, temperature has a very important influence

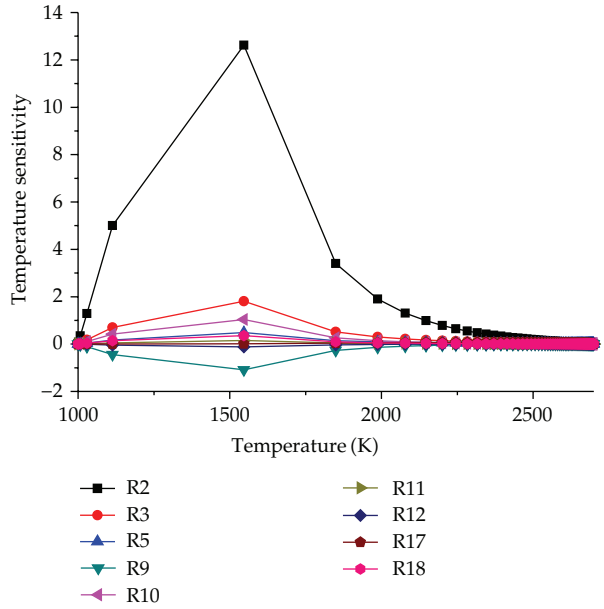

Figure 19: Temperature sensitivity for each reaction.

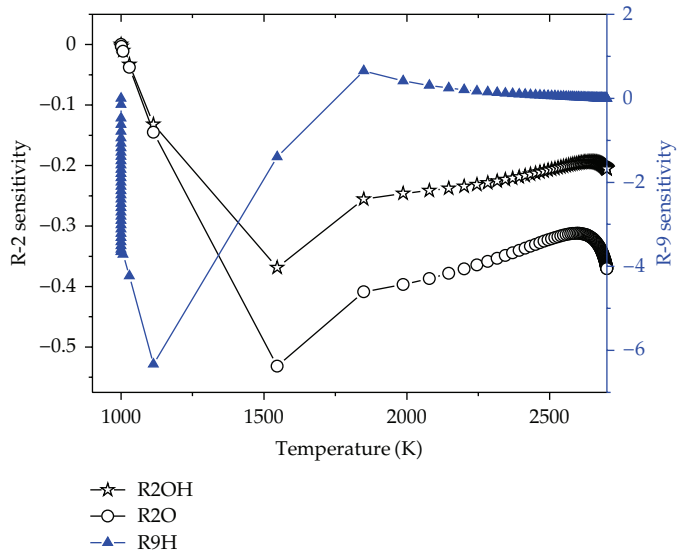

Figure 20: Temperature sensitivity for intermediate species of R2 and R9.

on reactions R2 and R9. According to formula (4.8), R2 is an exothermic reaction, so in ignition process, if we can improve the mixture temperature to 1550 K by a spark in a short time, the exothermic reaction R2 will occur immediately, and the heat will be released from R2 rapidly. So R2 is very important to ignition process. In contrast, reaction R9 possesses the largest negative temperature sensitivity coefficient in all the elementary reactions. It means that increasing its rate will lead to a lower temperature. So, reactions R2 and R9 dominate

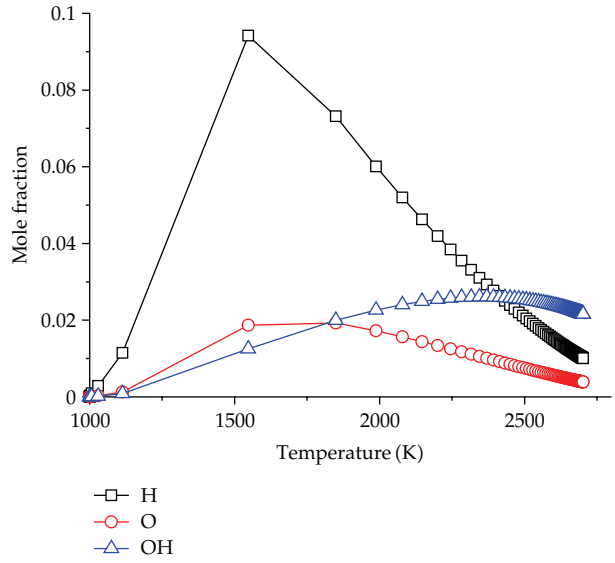

Figure 21: Profiles of intermediate species versus temperature.

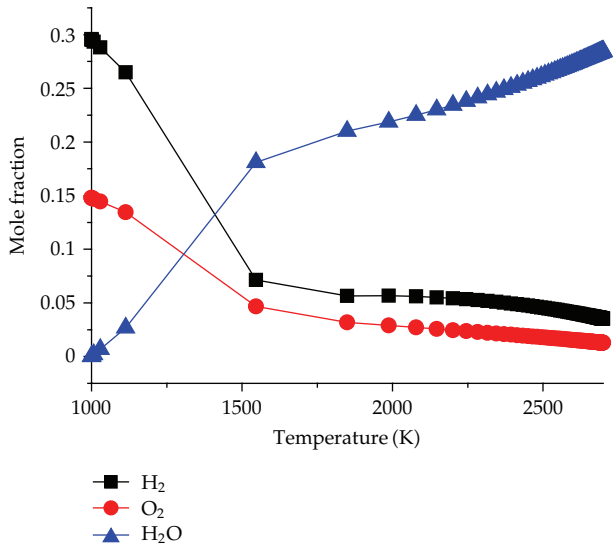

Figure 22: Profiles of reactants and production versus temperature.

the ignition and extinction processes. R9 ought to be the first reaction taking place in ignition process, and R2 ought to be the last one consider

$$\mathrm{OH} + \mathrm{O} \Longrightarrow \mathrm{O_2} + \mathrm{H} \tag{4.7}$$

$$\Delta h = [h(\mathrm{O_2}) + h(\mathrm{H})] - [h(\mathrm{O}) + h(\mathrm{OH})] = -70(\mathrm{kJ/mole}) \tag{4.8}$$

To investigate the influence of species concentration on chemistry reaction, the species sensitivity of intermediate species (H, O, and OH), reactants, and production were carried

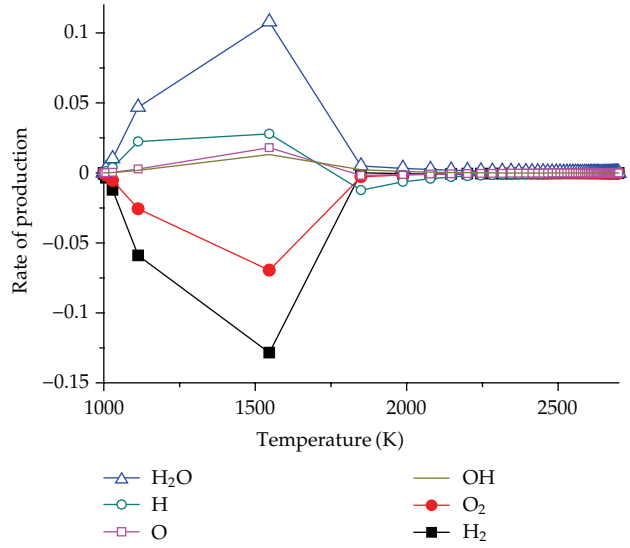

Figure 23: Rate of production versus temperature.

out. Figure 20 shows that to R2, the species sensitivity (O, OH) would decrease first and rise up later as temperature increases. When the temperature reaches 1550 K, the species sensitivity reaches the lowest value. It means that the species change rate reaches the maximum value. The H sensitivity of R9 reaches to the lowest value at 1120 K which is earlier than species O and OH, which indicates that reaction R9 ought to be taking place earlier than R2. Because in ignition process the fresh mixture must obtain heat from igniter source, the ignition will not be successful until the flame core accumulates enough heat. Figures 21 and 22 show that before 1550 K, the reactant (H_2, O_2) mole fraction will decline rapidly and the intermediate species and production concentration will rise greatly. It means that the endothermic reactions R1, R3, R5, and R9 take place immediately when the temperature rises from 1000 K to 1550 K. When the temperature exceeds 1550 K, the decreasing rate of species H_2 and O_2 is lower than that before 1550 K, which indicates that the flame was not ignited until $T = 1550$ K.

Figure 23 shows that the consumed rate of the reactant (O_2, H_2) increases rapidly before 1550 K and changes a little when the temperature reaches to 1850 K then remains unchanged. The same is done to intermediate species (O, OH, H) and production. It indicates that the ignition is successful after $T = 1550$ K, and the flame comes into being homeostasis after 1850 K.

Figure 24 shows the relationship between temperature sensitivity and equivalence ratio ($\Phi = 0.1 \sim 10.0$). It can be seen that the temperature sensitivity of reaction R2 will rise first and decrease later as equivalence ratio increases. The temperature sensitivity reaches to the peak value when equivalence ratio rises to 2. When equivalence ratio is lower than 0.1 or higher than 10, the chemistry reaction will not take place because it has exceeded the combustibility limit. Figure 25 shows that the temperature sensitivity of R9 will decrease first and increase later with the increasing equivalence ratio, and it will reach the lowest value when equivalence ratio reaches 1. It means that when equivalence ratio is 1, the mixture is most ignitable. In a word, people can control the chemistry reaction process, flame temperature, or ignition process by adjusting the mixture equivalence ratio.

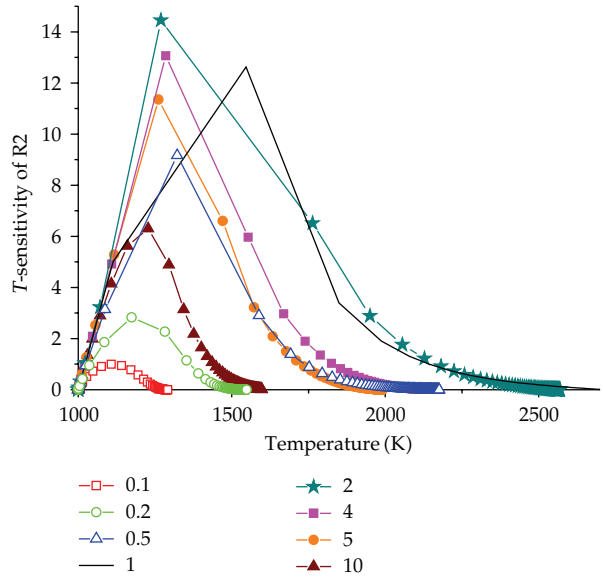

Figure 24: Temperature sensitivity coefficient of R2 versus equivalence ratio.

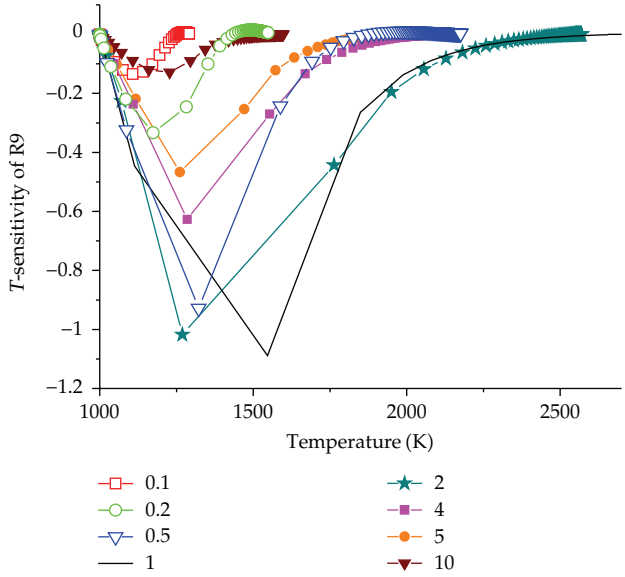

Figure 25: Temperature sensitivity coefficient of R9 versus equivalence ratio.

5. Conclusion

The numerical simulation on H_2 premixed flame in a bluff-body burner has been carried out. The H_2 flame ignition and extinction process is analyzed, and a function formula is summarized for H_2 RBL. The results showed that k-epsilon-C-PDF model is a reasonable method to capture H_2 RBL. There should be an optimal blockage ratio, which can stabilize the flame best. The flame will take an "M" shape with reaction fronts inside the CRZ

near the blow off condition. This research can provide theoretical instruction for bluff-body burner design, gas flow velocity control, fuel concentration matching, and the flame stability research. To systematically analyze the role of each elementary chemistry reaction taking place in the global combustion, CHEMKIN software was adopted to investigate the sensitivity of each elementary reaction. Other conclusions are as follows.

(1) When the blockage ratio remains unchanged, H_2 rich blowout limit is gas flow velocity's logarithmic function.

(2) When the gas flow velocity remains unchanged, H_2 rich blowout limit is blockage ratio's quadratic function.

(3) The fitting formula of H_2 rich blowout limit is $Y = a\lg V + b$ $(V \leq 50\,\mathrm{m/s})$, where, B is blockage ratio, $a = -0.02646 - 0.025088B + 0.027977B^2$, and $b = 0.75327 + 0.145B - 0.1625B^2$.

(4) A complete extinction process in a bluff-body burner requires three phases, the suddenly decline of the temperature in the main stream, the energy dissipation from the recirculation zone to the main stream, and the flame complete extinction.

(5) Reactions R2 and R9 possess the largest positive and negative temperature sensitivity. Increasing the rate of R2 will lead to a higher temperature, and increasing the rate of R9 will lead to a lower temperature. When equivalence ratio is 1, the mixture is most ignitable. The critical ignition temperature is 1550 K. Temperature has a very important influence on reactions R2 and R9.

References

[1] S. J. Shanbhogue, S. Husain, and T. Lieuwen, "Lean blowoff of bluff body stabilized flames: scaling and dynamics," *Progress in Energy and Combustion Science*, vol. 35, no. 1, pp. 98–120, 2009.

[2] P. Eriksson, "The Zimont TFC model applied to premixed bluff body stabilized combustion using four different rans turbulence models," in *Proceedings of the Turbo Expo: Power for Land, Sea, and Air Conference*, pp. 353–361, Montreal, Canada, May 2007.

[3] S. M. Frolov, V. Y. Basevich, and A. A. Belyaev, "Mechanism of turbulent flame stabilization on a bluff body," *Chemical Physics Reports*, vol. 18, no. 8, pp. 1495–1516, 2000.

[4] F. H. Wright, "Bluff-body flame stabilization: blockage effects," *Combustion and Flame*, vol. 3, pp. 319–337, 1959.

[5] J. R. Dawson, R. L. Gordon, J. Kariuki, E. Mastorakos, A. R. Masri, and M. Juddoo, "Visualization of blow-off events in bluff-body stabilized turbulent premixed flames," *Proceedings of the Combustion Institute*, vol. 33, no. 1, pp. 1559–1566, 2011.

[6] P. Griebel, E. Boschek, and P. Jansohn, "Lean blowout limits and NOx emissions of turbulent, lean premixed, hydrogen-enriched methane/air flames at high pressure," *Journal of Engineering for Gas Turbines and Power*, vol. 129, no. 2, pp. 404–410, 2007.

[7] R. W. Schefer, "Hydrogen enrichment for improved lean flame stability," *International Journal of Hydrogen Energy*, vol. 28, no. 10, pp. 1131–1141, 2003.

[8] R. S. Barlow, J. H. Frank, A. N. Karpetis, and J. Y. Chen, "Piloted methane/air jet flames: transport effects and aspects of scalar structure," *Combustion and Flame*, vol. 143, no. 4, pp. 433–449, 2005.

[9] E. Giacomazzi, V. Battaglia, and C. Bruno, "The coupling of turbulence and chemistry in a premixed bluff-body flame as studied by LES," *Combustion and Flame*, vol. 138, no. 4, pp. 320–335, 2004.

[10] C. X. Lin and R. J. Holder, "Reacting turbulent flow and thermal field in a channel with inclined bluff body flame holders," *Journal of Heat Transfer*, vol. 132, no. 9, pp. 1–11, 2010.

[11] W. W. Kim, J. J. Lienau, P. R. Van Slooten, M. B. Colket, R. E. Malecki, and S. Syed, "Towards modeling lean blow out in gas turbine flameholder applications," *Journal of Engineering for Gas Turbines and Power*, vol. 128, no. 1, pp. 40–48, 2006.

[12] W. P. Jones and V. N. Prasad, "Large eddy simulation of the sandia flame series (D-F) using the Eulerian stochastic field method," *Combustion and Flame*, vol. 157, no. 9, pp. 1621–1636, 2010.

[13] Ansys Fluent 12.0 Documentation.
[14] F. Bisetti and J. Y. Chen, *LES of Sandia Flame D with Eulerian PDF and Finite-Rate Chemistry*, Combustion Modeling, Combustion Processes Laboratories, Berkeley, Calif, USA, 2005.
[15] R. P. Lindstedt, S. A. Louloudi, and E. M. Váos, "Joint scalar probability density function modeling of pollutant formation in piloted turbulent jet diffusion flames with comprehensive chemistry," *Proceedings of the Combustion Institute*, vol. 28, no. 1, pp. 149–156, 2000.
[16] S. M. Correa and S. B. Pope, "Comparison of a monte carlo PDF/finite-volume mean flow model with bluff-body raman dsata," in *Proceedings of the 24th Symposium International on Combustion*, pp. 279–285, The Combustion Institute, 1992.
[17] S. M. S. El-feky and A. Penninger, "Study of flammability lean limit for a bluff body stabilized flame," *Periodica Polytechnica, Mechanical Engineering*, vol. 38, no. 1, pp. 33–45, 1994.
[18] Reaction Design, "Theory manual," CHEMKIN Release 4. 1. 1.
[19] Y. T. Liang and W. Zeng, "Kinetic simulation of gas explosion in constant volume bomb," *Journal of Combustion Science and Technology*, vol. 16, no. 4, pp. 375–381, 2010.